Molecular Therapy
Original Article

# circEHBP1 promotes lymphangiogenesis and lymphatic metastasis of bladder cancer via miR-130a-3p/TGFβR1/VEGF-D signaling

Jiang Zhu,[1,7] Yuming Luo,[2,7] Yue Zhao,[3,7] Yao Kong,[2,7] Hanhao Zheng,[4,5] Yuting Li,[2] Bowen Gao,[6] Le Ai,[1] Hao Huang,[4,5] Jian Huang,[4,5] Zhihua Li,[1] and Changhao Chen[4,5]

[1]Department of Oncology, Sun Yat-sen Memorial Hospital, Guangzhou, Guangdong, P.R. China; [2]Department of General Surgery, Guangdong Provincial People's Hospital, Guangdong Academy of Medical Sciences, Guangzhou, Guangdong, P.R. China; [3]Department of Interventional Oncology, The First Affiliated Hospital of Sun Yat-sen University, Guangzhou, Guangdong, P.R. China; [4]Department of Urology, Sun Yat-sen Memorial Hospital, Sun Yat-sen University, Guangzhou, Guangdong, P.R. China; [5]Guangdong Provincial Key Laboratory of Malignant Tumor Epigenetics and Gene Regulation, Sun Yat-sen Memorial Hospital, State Key Laboratory of Oncology in South China, Guangzhou, Guangdong, P.R. China; [6]Department of Pancreatobiliary Surgery, Sun Yat-sen Memorial Hospital, Guangzhou, Guangdong, P.R. China

**Lymphatic metastasis constitutes a leading cause of recurrence and mortality in bladder cancer. Accumulating evidence indicates that lymphangiogenesis is indispensable to trigger lymphatic metastasis. However, the specific mechanism is poorly understood. In the present study, we revealed a pathway involved in lymphatic metastasis of bladder cancer, in which a circular RNA (circRNA) facilitated lymphangiogenesis in a vascular endothelial growth factor C (VEGF-C)-independent manner. Novel circRNA circEHBP1 was markedly upregulated in bladder cancer and correlated positively with lymphatic metastasis and poor prognosis of patients with bladder cancer. circEHBP1 upregulated transforming growth factor beta receptor 1 (*TGFBR1*) expression through physically binding to miR-130a-3p and antagonizing the suppression effect of miR-130a-3p on the 3′ UTR region of *TGFBR1*. Subsequently, circEHBP1-mediated TGFβR1 overexpression activated the TGF-β/SMAD3 signaling pathway, thereby promoting the secretion of VEGF-D and driving lymphangiogenesis and lymphatic metastasis in bladder cancer. Importantly, administration of VEGF-D neutralizing antibodies remarkably blocked circEHBP1-induced lymphangiogenesis and lymphatic metastasis *in vivo*. Our findings highlighted that the circEHBP1/miR-130a-3p/TGFβR1/VEGF-D axis contributes to lymphangiogenesis and lymphatic metastasis of bladder cancer independent of VEGF-C, which might lead to the development of circEHBP1 as a potential biomarker and promising therapeutic target for lymphatic metastasis in bladder cancer.**

## INTRODUCTION

Bladder cancer (BCa) is one of the ten most common malignancies, with an estimated 430,000 new diagnosed patients and over 170,000 deaths worldwide annually.[1] The presence of lymph node (LN) metastasis is a potently pathological predictor of poor prognosis in BCa, accompanied by a reduction of the average 5-year survival rate to merely 18.6%.[2,3] Emerging evidence illustrates that lymphangiogenesis, which refers to the formation of new lymphatic vessels from the preexisting lymphatics, intratumorally and peritumorally, promotes the process of LN metastasis.[4,5] Despite the crucial role that lymphangiogenesis plays in LN metastasis of human cancer, the underlying mechanism of lymphangiogenesis in BCa is poorly understood.

Lymphangiogenesis is stimulated by identified lymphangiogenic factors, in particular, vascular endothelial growth factor (VEGF)-C and VEGF-D, which are dedicated to the growth of lymphatic vessels.[6] Recently, VEGF-D was validated to facilitate lymphangiogenesis and LN metastasis in multiple cancers.[7] In addition, it has been reported that VEGF-D neutralizing antibodies could decrease the spread of tumor cells to LNs by inhibiting the dilation of the lymphatic collecting duct.[8] Therefore, VEGF-D might be a novel indicator for LN metastasis in malignant tumors, and the role of VEGF-D in LN metastasis of BCa should be investigated urgently.

The transforming growth factor beta receptor 1 (TGFβR1), a serine/threonine kinase receptor, mainly works as the central signal

Received 24 April 2020; accepted 21 January 2021;
https://doi.org/10.1016/j.ymthe.2021.01.031.

[7]These authors contributed equally

**Correspondence:** Changhao Chen, MD, PhD, Department of Urology, Sun Yat-sen Memorial Hospital, 107 Yanjiangxi Road, Yuexiu District, Guangzhou, Guangdong 510120, P.R. China.
**E-mail:** chenchh53@mail.sysu.edu.cn
**Correspondence:** Jian Huang, MD, PhD, Department of Urology, Sun Yat-sen Memorial Hospital, 107 Yanjiangxi Road, Yuexiu District, Guangzhou, Guangdong 510120, P.R. China.
**E-mail:** huangj8@mail.sysu.edu.cn
**Correspondence:** Zhihua Li, MD, Department of Medical Oncology, Sun Yat-sen Memorial Hospital, 107 Yanjiangxi Road, Yuexiu District, Guangzhou, Guangdong 510120, P.R. China.
**E-mail:** lzhdoct@163.com

 

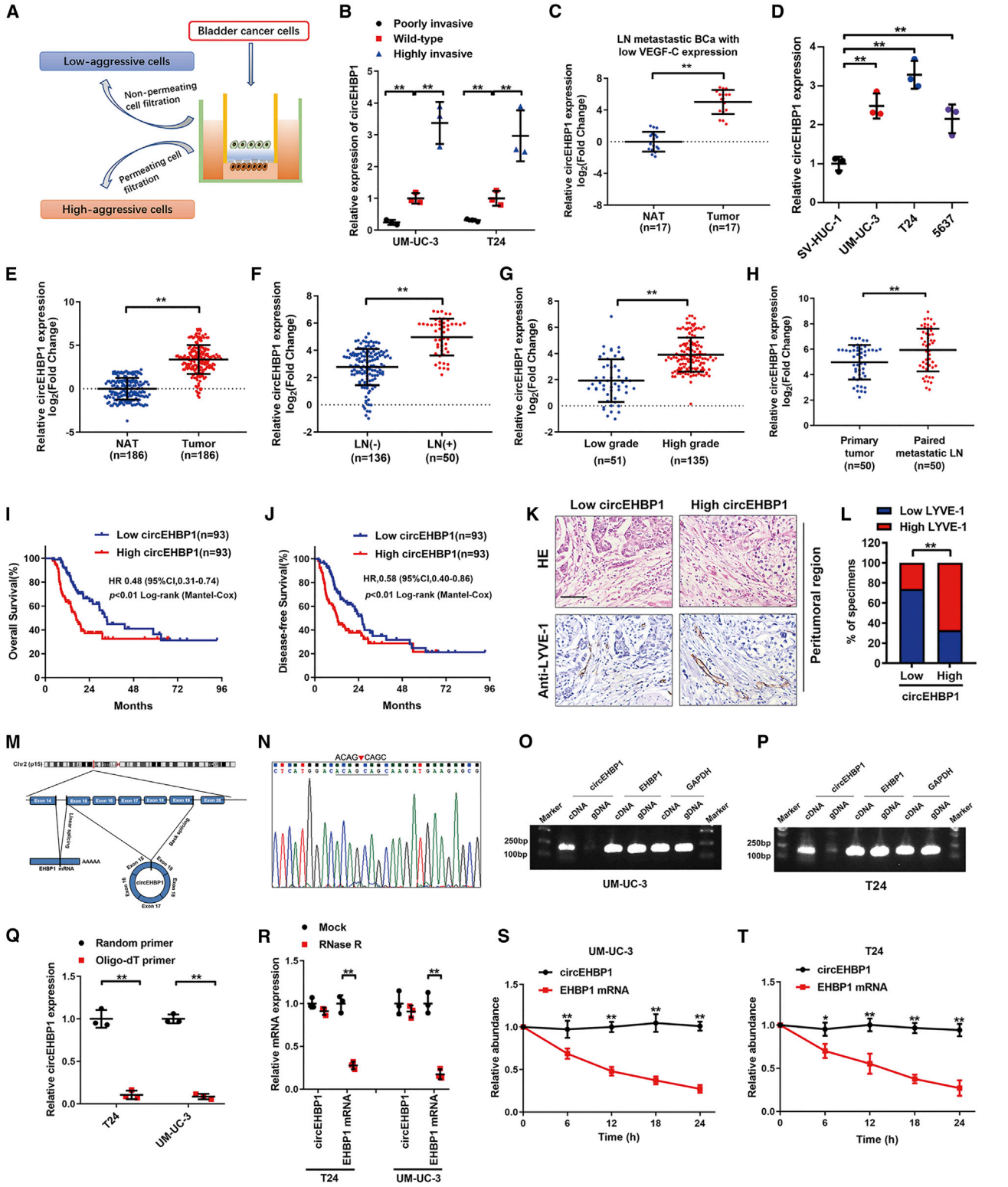


*(legend on next page)*

transducer of the TGF-β signaling pathway by phosphorylating the downstream protein SMAD2/3 and promotes the malignant progression of cancers.[9] Numerous studies have verified that TGFβR1 acts as a critical metastatic promoter to enhance the colonization of distant organs by cancer cells.[10] Further analysis revealed that TGFβR1 induced LN metastasis of human cancers and that blocking the TGF-β signaling pathway was a potential target to treat cancers.[11,12] Nevertheless, the precise regulatory mechanism that induces TGFβR1 to promote lymphangiogenesis and LN metastasis of BCa remains unclear.

Circular RNAs (circRNAs), a class of single-stranded molecules with development-specific expression patterns, are characterized by a covalently closed structure and generated from the back-splicing of pre-mRNA transcripts. Differing from linear RNAs, circRNAs contain neither 5′–3′ polarity nor a polyadenylation tail.[13,14] Accumulating studies have reported that circRNAs are widely detected in a variety of cancers and play an indispensable regulatory role in tumor development and progression.[15,16] Herein, we report a novel circRNA, circEHBP1 (hsa_circ_0005552), which was markedly upregulated in BCa and correlated positively with the prognosis of patients with BCa. circEHBP1 overexpression induced lymphangiogenesis and LN metastasis of BCa *in vitro* and *in vivo*. Mechanistically, circEHBP1 overexpression promoted TGFβR1 expression by attenuating miR-130a-3p to activate the TGF-β/SMAD3 signaling pathway, further elevating VEGF-D secretion and ultimately facilitating lymphangiogenesis and LN metastasis of BCa. Our findings revealed a VEGF-C-independent mechanism of circEHBP1-mediated lymphangiogenesis of BCa and implied circEHBP1 is a potential therapeutic target to treat LN metastasis in BCa.

## RESULTS

### circEHBP1 is correlated with LN metastasis in BCa

To identify the critical circRNAs involved in the LN metastasis of BCa, 47 upregulated circRNAs (fold change $\geq$ 2.0 and $p < 0.05$) were screened from RNA sequencing data (GEO: GSE77661)[17] of BCa tissue and normal adjacent tissue (NAT). Then, the elevated circRNAs were validated in the previously established invasion model of BCa cell lines, and 23 invasion-related circRNAs were selected (Figures 1A and 1B). Previously, we verified that VEGF-C is a key inducer for LN metastasis of BCa.[18] However, a few patients with BCa with LN metastasis possess low VEGF-C expression,[19,20] indicating the presence of a VEGF-C-independent mechanism for LN metastasis of BCa. Thus, the top 10 ranked circRNAs from the above screening according to their fold changes were further evaluated in 17 LN-positive BCa tissues with low VEGF-C expression, which showed that circEHBP1 (hsa_circ_0005552) was the most significantly upregulated circRNA; therefore, we chose circEHBP1 for further study (Figure 1C; Table S1).

Next, we studied the role of circEHBP1 in BCa. First, we found that higher circEHBP1 levels were detected in UM-UC-3, T24, and 5637 cells (BCa cells) compared with those in SV-HUC-1 cells (human uroepithelial cells) (Figure 1D). Further analysis in a cohort of 186 cases of BCa showed that circEHBP1 was overexpressed in BCa tissues and was associated positively with LN metastasis and the pathological grades of patients with BCa (Figures 1E–1G; Figures S1A–S1C; Table 1). Moreover, circEHBP1 expression was higher in metastatic LNs compared with that in primary tumors (Figure 1H; Figure S1D). Kaplan-Meier analysis revealed that circEHBP1 expression associated negatively with overall survival (OS) and disease-free survival (DFS) in patients with BCa (Figures 1I and 1J). Univariate and multivariate analyses indicated that poor prognosis of patients with BCa was independently affected by circEHBP1 (Tables S2 and S3). *In situ* hybridization (ISH) analysis showed that the lymphatic vessel density (LVD) in BCa tissues correlated positively with circEHBP1 expression (Figures 1K and 1L). Taken together, these results indicated that circEHBP1 is associated with LN metastasis of BCa.

### Characteristics of circEHBP1 in BCa cells

circEHBP1 was derived from exon 15 to exon 19 of the *EHBP1* gene (encoding EH domain binding protein 1) with a length of 751 nucleotides (nt), in which the back-spliced junction was confirmed using Sanger sequencing (Figures 1M and 1N). Moreover, circEHBP1 could only be amplified from the complementary DNA (cDNA) rather than the genomic DNA (gDNA) (Figures 1O and 1P). Compared with the results

**Figure 1. circEHBP1 is upregulated in LN metastasis of BCa**

(A) Schematic illustration of the modeling of poorly invasive and highly invasive cell sublines from BCa. (B) Relative expression of circEHBP1 in poorly invasive, wild-type, and highly invasive UM-UC-3 and T24 cell sublines. (C) circEHBP1 level analyzed by quantitative real-time RT-PCR in a 17-case cohort of LN metastatic BCa tissues with low VEGF-C expression paired with corresponding NATs. The Mann-Whitney U test was employed. (D) Relative expression of circEHBP1 in BCa cell lines and SV-HUC-1 was detected using quantitative real-time RT-PCR . (E) Quantitative real-time RT-PCR for the circEHBP1 expression in a 186-case cohort of BCa tissues paired with corresponding NATs. The Mann-Whitney U test was employed. (F and G) Quantitative real-time RT-PCR analysis of circEHBP1 expression in 186 BCa tissues with respect to LN status (F) and pathological grade (G). The Mann-Whitney U test was employed. (H) circEHBP1 expression in primary BCa samples and paired metastatic LNs was detected by quantitative real-time RT-PCR . The Mann-Whitney U test was employed. (I and J) Kaplan-Meier survival curves for OS (I) and DFS (J) of low circEHBP1 level versus high circEHBP1 level in patients with BCa. The median expression level of circEHBP1 was taken as the cutoff value. (K and L) Representative images (K) and proportion (L) for IHC staining showing the LVD stained with anti-LYVE-1 in the BCa tissues with differential circEHBP1 expression. Scale bar, 50 μm. (M) Schematic illustrating the genetic locus of the *EHBP1* gene and the circEHBP1 derived from exon 15 to 19 of EHBP1. (N) Sanger sequencing for the back-splice junction site of circEHBP1. (O and P) PCR with an agarose gel electrophoresis assay for circEHBP1 and EHBP1 in the cDNA and gDNA of UM-UC-3 (O) or T24 (P) cells. GAPDH was applied for NC. (Q) Relative circEHBP1 expression was evaluated by quantitative real-time RT-PCR using random primers or oligo-dT primers. (R) circEHBP1 and EHBP1 mRNA expression analyzed by quantitative real-time RT-PCR following RNase R treatment in UM-UC-3 and T24 cells. (S and T) Actinomycin D assay to assess the stability of circEHBP1 and EHBP1 mRNA in UM-UC-3 (S) or T24 (T) cells at the indicated time points. Two-tailed Student's t test or 1-way analyses of variance were used for significance level, and Dunnett's test was used to perform multiple comparisons. Error bars indicate the standard deviations. *$p < 0.05$, **$p < 0.01$.

**Table 1. Correlation between circEHBP1 expression and clinicopathologic characteristics of BC patients**

| | | circEHBP1 expression level | | |
|---|---|---|---|---|
| Characteristics | No. of cases | Low | High | p value[a] |
| Total cases | 186 | 93 | 93 | |
| Gender | | | | |
| Male | 132 | 64 | 68 | 0.51794 |
| Female | 54 | 29 | 25 | |
| Age, years | | | | |
| <65 | 76 | 38 | 38 | 1 |
| ≥65 | 110 | 55 | 55 | |
| T stage | | | | |
| T1 | 46 | 24 | 22 | 0.73341 |
| T2-4 | 140 | 69 | 71 | |
| Lymphatic metastasis | | | | |
| Negative | 136 | 84 | 52 | 0.001** |
| Positive | 50 | 9 | 41 | |
| Grade | | | | |
| Low | 51 | 41 | 10 | 0.001** |
| High | 135 | 52 | 83 | |

T stage, tumor stage; grade, tumor node metastasis stage.
[a]Chi-square test, **$p < 0.01$.

using random primers, circEHBP1 expression was scarcely detected using oligo-dT primers, indicating that circEHBP1 lacked a poly-A tail (Figure 1Q). circRNAs exhibit higher stability than their linear counterparts; therefore, we further studied the stability of circEHBP1. The results showed that circEHBP1 was resistant to RNase R compared with linear EHBP1 mRNA (mEHBP1) or linear control GAPDH (Figure 1R; Figures S1E and S1F). The half-life of circEHBP1 was longer than that of mEHBP1 after treatment with actinomycin D, which blocks *de novo* RNA synthesis (Figures 1S and 1T). The above results illustrated that circEHBP1, as a circRNA, possesses high stability.

### circEHBP1 promotes lymphangiogenesis of BCa *in vitro*

Lymphangiogenesis is identified as a considerable step of LN metastasis; therefore, we further explored the effect of circEHBP1 on lymphangiogenesis of BCa *in vitro*. circEHBP1 was successfully downregulated through transfection with small interfering RNAs (siRNAs) that targeted the head-to-tail splicing region of circEHBP1 and upregulated after transfection with circEHBP1-overexpressing plasmid. No significant changes in mEHBP1 expression were observed (Figures 2A–2D). The *in vitro* assay showed that circEHBP1 knockdown in UM-UC-3 and T24 cells dramatically abolished their ability to induce tube formation and migration of human lymphatic endothelial cells (HLECs), while circEHBP1 overexpression facilitated UM-UC-3 and T24 cells to drive HLEC tube formation and migration (Figures 2E–2P). In addition, although Cell Counting Kit-8 (CCK-8) and colony formation assays showed that circEHBP1 knockdown inhibited the proliferation of UM-UC-3 and T24 cells and circEHBP1 overexpression promoted their proliferation ability (Figures S1G–S1N), the alteration of circEHBP1 expression had no significant effect on the invasiveness of BCa cells, which further verified that circEHBP1 played a crucial role in LN metastasis through facilitating the lymphangiogenesis. Collectively, these findings suggested that circEHBP1 triggers lymphangiogenesis of BCa *in vitro*.

### circEHBP1 facilitates LN metastasis of BCa *in vivo*

To further investigate the role of circEHBP1 in LN metastasis *in vivo*, we constructed a popliteal lymph node metastatic model through the inoculation of luciferase-labeled vector or circEHBP1-overexpressing UM-UC-3 cells into the right footpads of nude mice (Figure 3A). LN metastatic status was measured when the footpad tumors reached about 200 $mm^3$. The *in vivo* imaging systems (IVIS) results indicated that the fluorescence intensity was remarkably increased in the circEHBP1-overexpressing group, and the volume of popliteal LNs was larger after circEHBP1 overexpression (Figures 3B–3E). Furthermore, the LN metastatic rate was higher in the circEHBP1-overexpressing group compared with that of the control group (Figure 3F). The ISH assay showed that circEHBP1 improved LVD in the primary tumor tissues, and survival analysis suggested that circEHBP1 shortened the survival of the mice (Figures 3G–3I). Taken together, these results indicated that circEHBP1 facilitates LN metastasis of BCa *in vivo*.

### circEHBP1 sponges miR-130-3p in BCa cells

Given that the distinct function of RNAs is based upon their subcellular localization, we next analyzed the localization of circEHBP1 in BCa cells. Fluorescence *in situ* hybridization (FISH) and subcellular fractionation assays demonstrated that circEHBP1 was primarily located in the cytoplasm of BCa cells (Figures 4A and 4B; Figure S2A). Cytoplasm-located circRNAs contain multiple microRNA (miRNA)-binding sites and mainly act as miRNA sponges.[21,22] Therefore, 10 candidate miRNAs that potentially bound to circEHBP1 were predicted using RegRNA 2.0 (http://regrna2.mbc.nctu.edu.tw/)[23] (Figure 4C). Only miR-130a-3p was enriched by circEHBP1 in an RNA pull-down assay (Figures 4D and 4E). The miR-130a-3p binding site of circEHBP1 was predicted using RNAalifold (http://rna.tbi.univie.ac.at/) and then mutated to conduct dual-luciferase reporter assays (Figures 4F and 4G). The result revealed that the luciferase activity of circEHBP1-wild-type (WT) was significantly reduced by miR-130a-3p, while circEHBP1-mut was not affected, supporting that this specific region was essential for the sponging effect of circEHBP1 on miR-130a-3p (Figure 4H; Figure S2B). Consistently, a pull-down assay with a biotin-labeled miR-130a-3p probe found that circEHBP1 was captured by miR-130a-3p (Figure 4I). Moreover, a FISH assay showed the colocalization of circEHBP1 and miR-130a-3p in the cytoplasm of UM-UC-3 and T24 cells (Figure 4J). Collectively, these findings verified that circEHBP1 sponges miR-130-3p in BCa.

### miR-130a-3p suppresses lymphangiogenesis of BCa

Next, we investigated the effect of miR-130a-3p on the lymphangiogenesis of BCa. First, we found that miR-130a-3p expression was

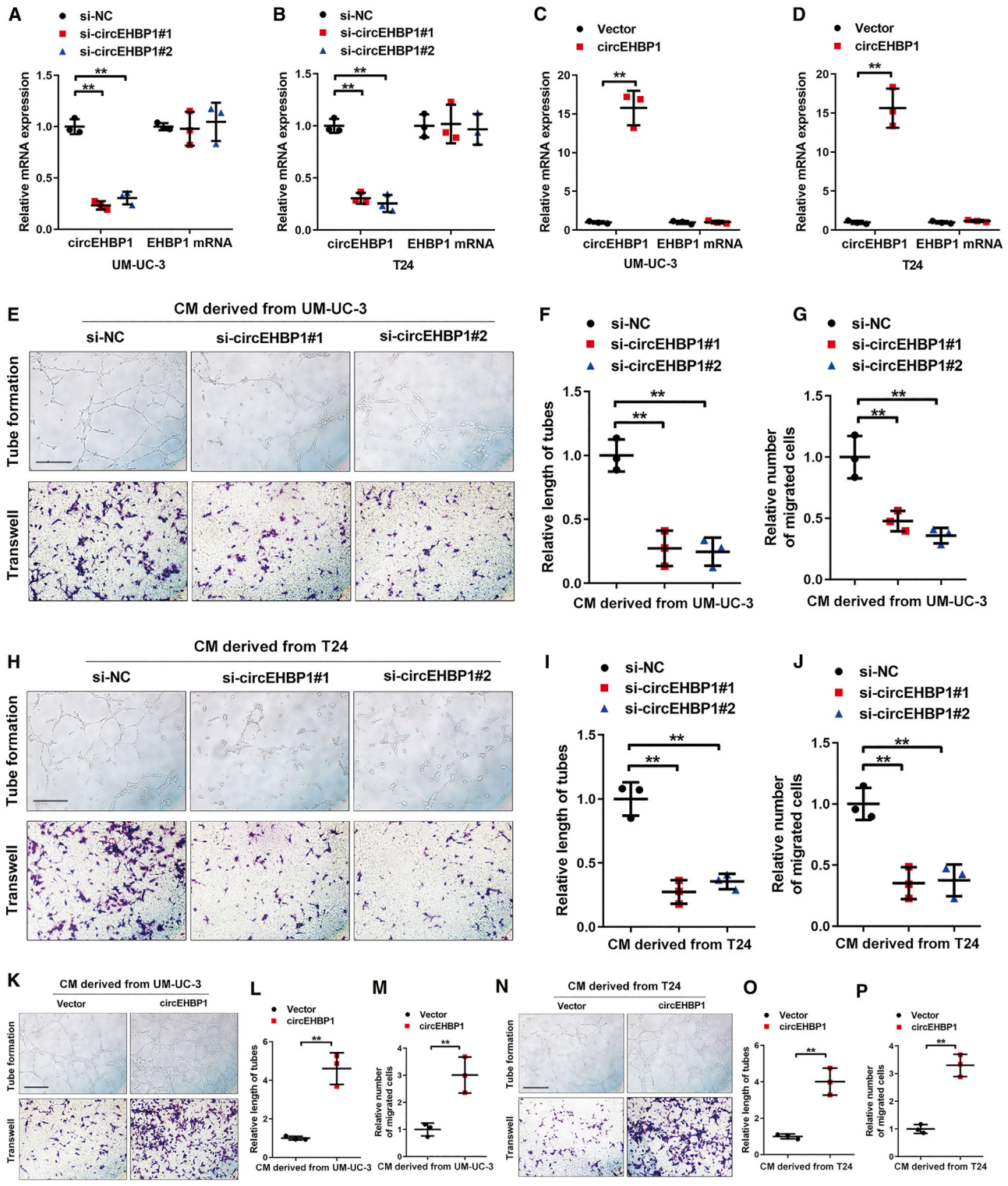


**Figure 2. circEHBP1 promotes lymphangiogenesis of BCa *in vitro***

(A–D) circEHBP1 and *EHBP1* level were assessed using quantitative real-time RT-PCR in circEHBP1 knockdown (A and B), circEHBP1 overexpression (C and D), and paired control BCa cells. (E–J) Representative images (E and H) and quantification of tube formation (F and I) and Transwell migration (G and J) by HLECs that were cultured with the

*(legend continued on next page)*

downregulated in UM-UC-3, T24, and 5637 cells compared with that in SV-HUC-1 cells (Figure S2C). miR-130a-3p expression was dramatically downregulated by an miR-130a-3p inhibitor and was successfully upregulated by an miR-130a-3p mimic (Figures S2D–S2G). We found that incubation with the conditioned media from miR-130a-3p-silencing UM-UC-3 and T24 cells enhanced the tube formation and migration ability of HLECs, while miR-130a-3p overexpression reduced the ability of UM-UC-3 and T24 cells to induce lymphangiogenesis (Figures 5A–5D). The above results demonstrated the suppressive effect of miR-130a-3p on lymphangiogenesis in BCa.

### circEHBP1 upregulates TGFβR1 to activate the TGF-β/SMAD signaling pathway in BCa

To explore the downstream targets of miR-130a-3p, TargetScan (http://www.targetscan.org/)[24] and miRTarBase (http://mirtarbase.mbc.nctu.edu.tw/)[25] were applied, and the predicted genes were intersected to acquire 76 genes for the further analysis in the Kyoto Encyclopedia of Genes and Genomes (KEGG) database.[26] The results showed that the TGF-β signaling pathway ranked highest among the enriched pathways (Figures S3A and S3B). Furthermore, quantitative real-time reverse transcription PCR (RT-PCR) and western blotting analysis revealed that only TGFβR1 expression correlated negatively with miR-130a-3p (Figures S3C–S3J). miRNAs exert their regulatory roles by binding to the 3′ UTR region of target genes;[27] therefore, we analyzed the sequences of miR-130a-3p and *TGFBR1* 3′ UTR region and found specific sequences within the 3′ UTR region of *TGFBR1* that were complementary to miR-130a-3p (Figure 5E). Dual-luciferase assays revealed that the luciferase activity of *TGFBR1*-WT was notably reduced by miR-130a-3p, whereas no obvious change was found after mutating the miR-130a-3p binding site in the *TGFBR1* 3′ UTR (Figures 5F and 5G). Therefore, *TGFBR1* is the downstream target of miR-130a-3p.

Next, we investigated whether circEHBP1 regulated TGFβR1 expression. circEHBP1 knockdown suppressed TGFβR1 expression, while circEHBP1 overexpression upregulated TGFβR1 (Figures 5H and 5I; Figures S3K–S3N). Importantly, miR-130a-3p knockdown partially alleviated circEHBP1-silencing-induced *TGFBR1* suppression, indicating that circEHBP1 upregulated *TGFBR1* expression by sponging miR-130a-3p (Figures 5J–5L). TGFβR1 is a phosphorylase of the TGF-β/SMAD3 signaling pathway; we further evaluated the role of circEHBP1 in the TGF-β/SMAD3 signaling pathway. circEHBP1 knockdown inhibited SMAD3 phosphorylation and TGFβR1 expression, while circEHBP1 overexpression had the opposite effects, suggesting that circEHBP1 activated the TGF-β/SMAD3 signaling pathway (Figures 5M–5P). Furthermore, TGFβR1 knockdown successfully reversed circEHBP1-induced upregulation of SMAD3 phosphorylation and TGFβR1 expression, indicating that circEHBP1 activated the TGF-β/SMAD3 signaling pathway through upregulating TGFβR1 (Figures S3O and S3P). Taken together, these results indicated that circEHBP1 upregulates TGFβR1 expression and activates the TGF-β/SMAD3 signaling pathway in BCa.

### circEHBP1 drives lymphangiogenesis via a VEGF-D-dependent mechanism

VEGF-C is pivotal for the induction of lymphangiogenesis. Previously, we verified the essential role of VEGF-C in lymphangiogenesis of BCa.[28] Nevertheless, some patients with LN metastatic BCa exhibited low VEGF-C expression,[19,20] indicating the presence of a VEGF-C-independent mechanism of inducing lymphangiogenesis in BCa. VEGF-D has been reported to play a compensatory role in lymphatic sprouting in animals with VEGF-C deficiency.[29] Therefore, we explored whether VEGF-D was involved in circEHBP1-induced lymphangiogenesis of BCa. VEGF-D levels were reduced by downregulating circEHBP1 and enhanced by upregulating circEHBP1 in BCa cells (Figures 6A and 6B). Consistent results were also obtained using an enzyme-linked immunosorbent assay (ELISA), indicating that circEHBP1 regulates VEGF-D expression positively (Figures 6C and 6D). Furthermore, inhibiting the TGF-β/SMAD3 signaling pathway using the TGFβR1 inhibitor LY364947 significantly abrogated circEHBP1-mediated VEGF-D expression (Figures 6E–6H). Moreover, treatment with VEGF-D neutralizing antibodies weakened the tube formation and migration ability of HLECs induced by circEHBP1 (Figure 6I; Figures S4A–S4C). The *in vivo* assay showed that the circEHBP1-induced increase in the volume and metastatic ratio of LNs was reduced by neutralizing VEGF-D, accompanied by prolonged survival (Figures 6J–6L). Importantly, immunohistochemistry (IHC) analysis revealed that circEHBP1 overexpression significantly increased the VEGF-D expression and the quantities of lymphatic vessels in footpad tumors, which were decreased by VEGF-D neutralization (Figures 6M–6O). Thus, our findings illustrated that circEHBP1 drives lymphangiogenesis by activating the TGF-β/SMAD3 signaling pathway and increasing VEGF-D secretion in BCa.

### Clinical relevance of the circEHBP1/miR-130a-3p/*TGFBR1*/VEGF-D axis in patients with BCa

circEHBP1 mediates the miR-130a-3p/*TGFBR1*/VEGF-D axis and contributes to LN metastasis of BCa; therefore, we examined the clinical relevance of this regulatory axis in a cohort of 186 patients with BCa. The results showed that miR-130a-3p was downregulated and *SMAD3*, *TGFBR1*, and *VEGF-D* were upregulated in BCa tissues compared with NATs. Moreover, miR-130a-3p was correlated negatively with LN metastatic status and the pathological grade, while *TGFBR1* and *VEGF-D* overexpression were associated with the LN metastasis of patients with BCa, suggesting their crucial roles in LN metastasis of BCa (Figures 7A–7E; Figures S4D–S4F). In addition, Kaplan-Meier analysis revealed that miR-130a-3p overexpression was accompanied by longer OS and DFS in 186 patients with BCa

supernatant obtained from control or circEHBP1-silencing UM-UC-3 and T24 cells. Scale bars, 100 μm. (K–P) Representative images (K and N) and quantification of tube formation (L and O) and Transwell migration (M and P) by HLECs were cultured with the supernatant obtained from control or circEHBP1-overexpressing UM-UC-3 and T24 cells. Scale bars, 100 μm. Two-tailed Student's t test or 1-way analyses of variance were used to determine the significance level, and Dunnett's test was used for multiple comparisons. Error bars indicate the standard deviations. *$p < 0.05$, **$p < 0.01$.

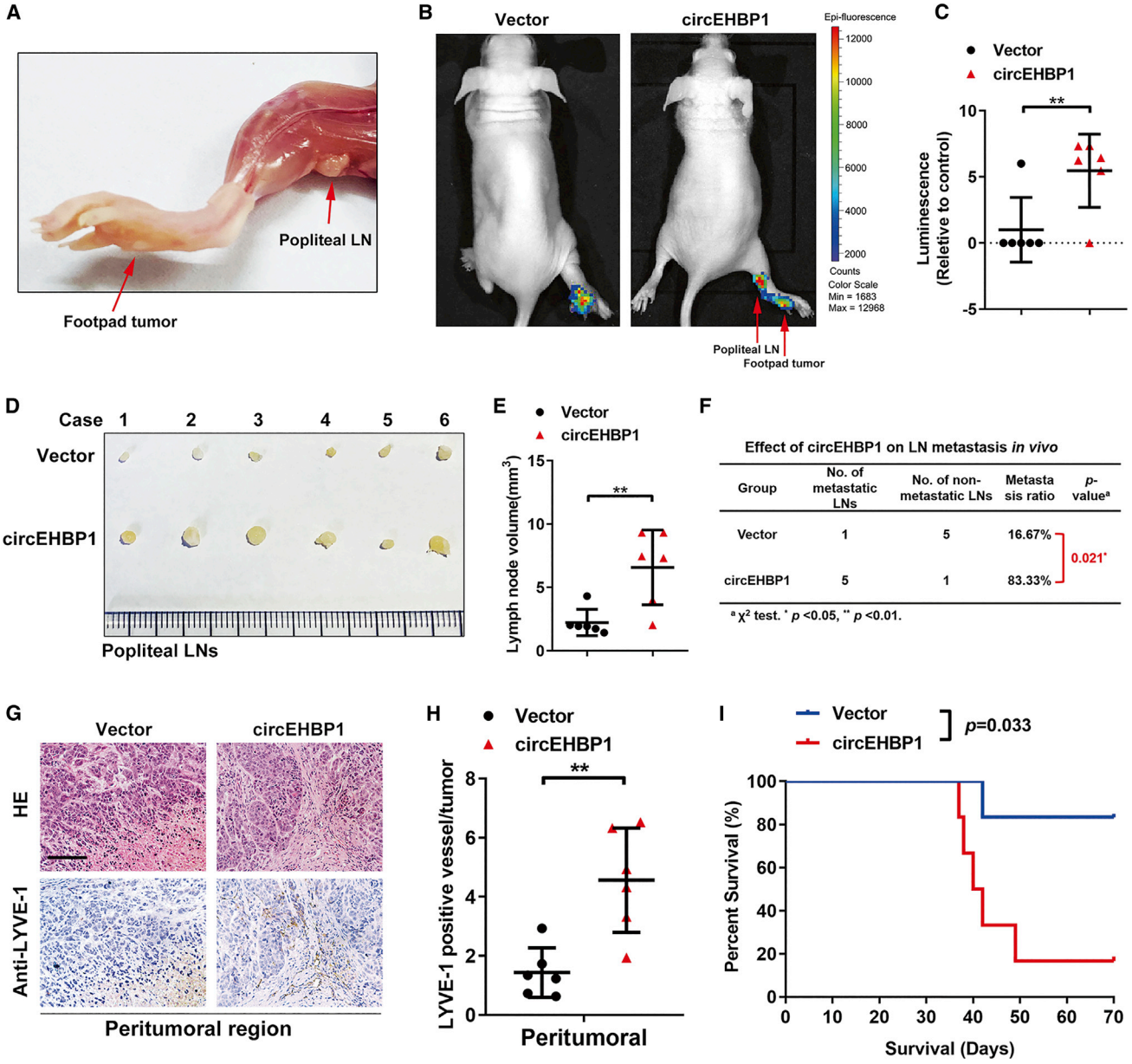


**Figure 3. circEHBP1 facilitate LN metastasis of BCa *in vivo***

(A) Representative images of popliteal LN metastasis in the nude mouse model. UM-UC-3 cells were inoculated into the right footpads of the nude mice, followed by the enucleation and evaluation of popliteal LNs. (B and C) Representative bioluminescence images (B) and histogram analysis (C) of popliteal LN metastasis from nude mice (n = 12) following overexpressing circEHBP1. (D and E) Representative images (D) of excised popliteal LNs from nude mice (n = 12) and the measurement of the LN volume (E). (F) The popliteal LN metastatic rate in all groups (n = 12). (G and H) Representative images (G) and histogram analysis (H) of IHC staining showing the LVD stained with anti-LYVE-1 in the mouse tissues with different circEHBP1 expression (n = 12). Scale bar, 50 μm. (I) Kaplan-Meier survival curves in all groups (n = 12). Two-tailed Student's t test or 1-way analyses of variance were used to determine the significance level and Dunnett's test for multiple comparisons. Error bars indicate standard deviations. *p < 0.05, **p < 0.01.

(Figures 7F and 7G). Furthermore, correlation analysis showed a negative correlation between circEHBP1 and miR-130a-3p in BCa and revealed that both *TGFBR1* and *VEGF-D* expression correlated positively with circEHBP1 expression and negatively with miR-130a-3p expression in BCa (Figures S4G–S4I; Figures 7H and 7I). Taken together, our results revealed that circEHBP1 induces the miR-130a-3p/*TGFBR1*/VEGF-D axis to facilitate LN metastasis in BCa.

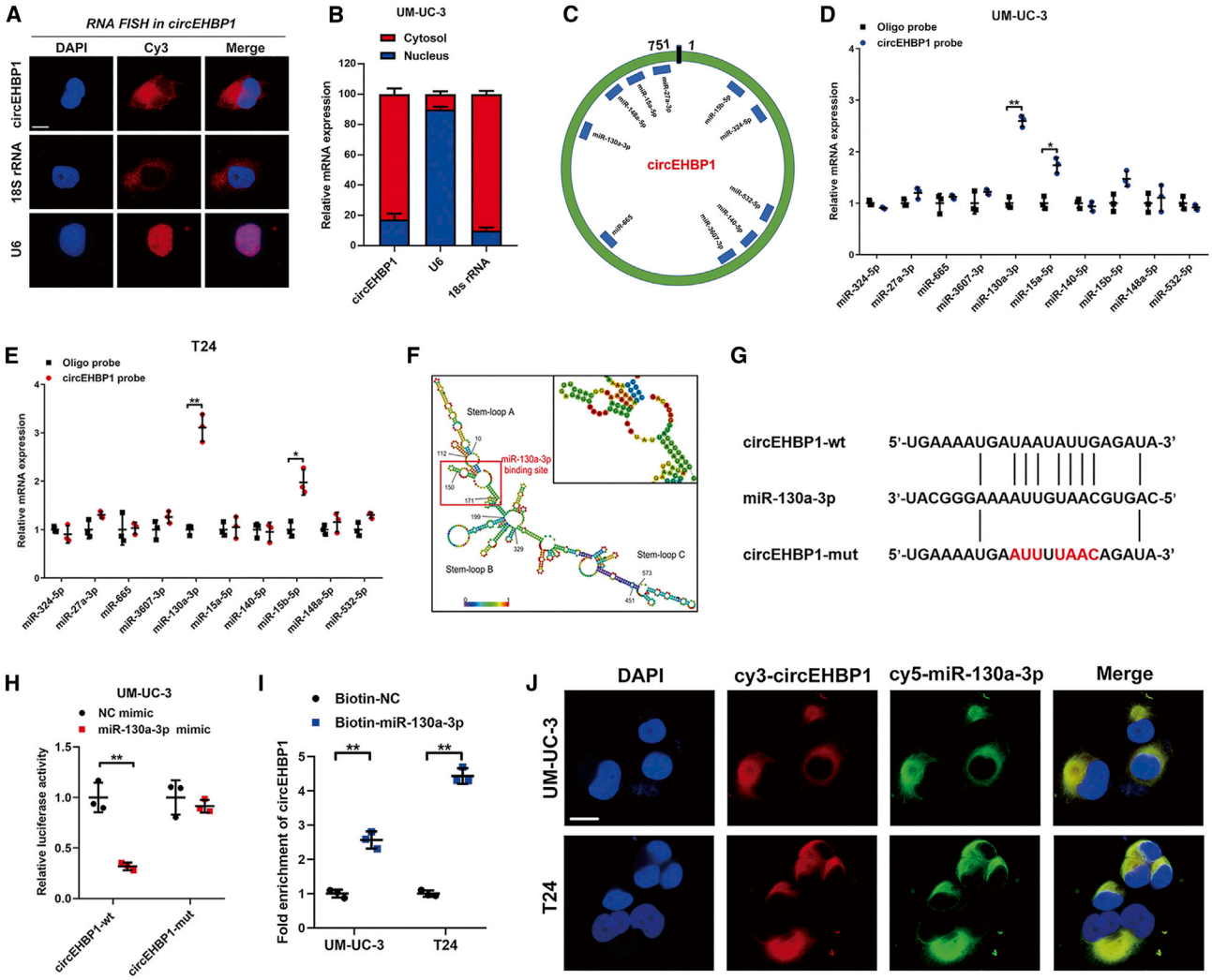


**Figure 4. circEHBP1 functions as a miR-130-3p sponge in BCa**

(A) The cellular localization of circEHBP1 was detected using a FISH assay. Scale bar, 100 μm. (B) The cellular localization of circEHBP1 in UM-UC-3 cells was confirmed using a subcellular fractionation assay. The nuclear control used U6 and the cytoplasmic control used 18S rRNA. (C) RegRNA 2.0 was used to predict the potential target miRNAs of circEHBP1. (D and E) Quantitative real-time RT-PCR analysis for the expression of ten predicted target miRNAs of circEHBP1 in UM-UC-3 (D) and T24 (E) cells. (F) RNAalifold was used to predict the secondary structure of circEHBP1. (G) Schematic illustrating the sequence alignment of circEHBP1 with miR-130a-3p. (H) The luciferase activities of the circEHBP1-wt plasmid or circEHBP1-mut plasmid quantified following transfecting NC mimic or miR-130a-3p mimics into UM-UC-3 cells. (I) Quantitative real-time RT-PCR analysis of the circEHBP1 captured by miR-130a-3p. (J) The co-localization of circEHBP1 and miR-130a-3p was detected by FISH assay. Scale bar, 100 μm. Two-tailed Student's t test or 1-way analyses of variance were used to determine the significance level, and Dunnett's test was used for multiple comparisons. Error bars indicate standard deviations. *$p < 0.05$, **$p < 0.01$.

## DISCUSSION

Lymphangiogenesis is believed to be indispensable for LN metastasis, which is responsible for the poor prognosis of patients with BCa.[30] Although VEGF-C is a key regulator in the lymphangiogenesis associated with human cancer, further investigation showed that a subset of patients with BCa with LN metastasis have a low level of VEGF-C;[19,20] however, there has been little research implicating a VEGF-C-independent mechanism of regulating LN metastasis in BCa. In the present study, we revealed a novel mechanism whereby circEHBP1 induces lymphangiogenesis of BCa in a VEGF-C-independent manner. circEHBP1 was overexpressed in BCa tissues and attenuated the endogenous inhibitory impact of miR-130a-3p on its downstream target TGFβR1, which further activated the TGF-β/SMAD3 signaling pathway to induce the expression of VEGF-D and promoted lymphangiogenesis and LN metastasis of BCa. To the best of our knowledge, this is the first report to illustrate a VEGF-C-independent mechanism regulated by circEHBP1 in lymphangiogenesis of BCa and might support circEHBP1 as a new intervention target for LN metastasis in BCa.

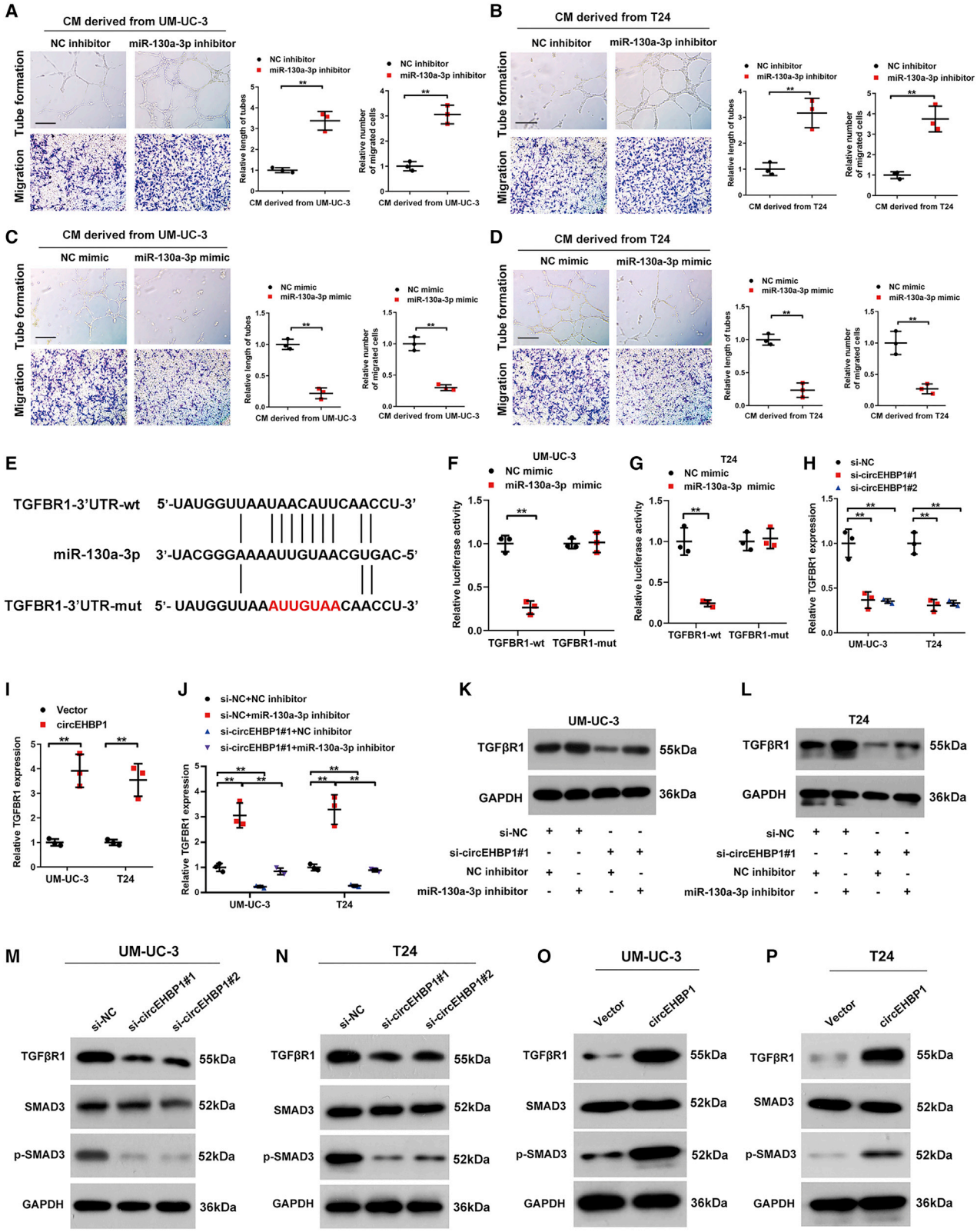


*(legend on next page)*

VEGF-D was reported to play a facilitative role in lymphangiogenesis in an *in vivo* model with low VEGF-C levels.[29,31] VEGF-D drives the formation of new lymphatic vessels via binding to vascular endothelial growth factor receptor 3 (VEGFR-3) and promoting LN metastasis.[32,33] However, the specific contribution of VEGF-D in lymphangiogenesis and LN metastasis of BCa remains unknown. In the present study, we demonstrated that VEGF-D overexpression contributes to lymphangiogenesis and LN metastasis of BCa, and blocking VEGF-D with neutralizing antibody markedly suppressed circEHBP1-induced lymphangiogenesis in BCa, indicating that VEGF-D functions as a vital inducer of lymphangiogenesis. Importantly, studies have reported a VEGF-D-driven induction of dilated lymphatic vessels and stimulation of LN metastasis in multiple tumors,[34,35] whereas how VEGF-D expression is regulated in LN metastasis of BCa remains elusive. In the present study, we confirmed that circEHBP1 induced the upregulation of VEGF-D, which promoted TGFβR1 overexpression and activation of the TGF-β/SMAD3 signaling pathway. Thus, our results revealed a regulatory mechanism of circEHBP1-induced VEGF-D expression in lymphangiogenesis and might provide insights into the regulation of LN metastasis in BCa.

Another valuable finding in our study is that TGFβR1 was remarkably upregulated in BCa with LN metastasis. TGFβR1 contributes to LN metastasis in several cancers by serving as a vital serine/threonine kinase receptor in the TGF-β/SMAD3 pathway.[36,37] Upregulation of TGFβR1 induced LN metastasis in breast cancer cells.[38] Moreover, the application of a TGFβR1 inhibitor suppressed lymphangiogenesis and LN metastasis in pancreatic cancer.[39] However, whether TGFβR1 is involved in the progression of LN metastasis in BCa remains unknown. In this study, we showed that the expression of *TGFBR1* was inhibited by miR-130a-3p via binding to the 3′ UTR of *TGFBR1*. circEHBP1 antagonized the inhibition of *TGFBR1* by miR-130a-3p and activated the TGF-β/SMAD3 signaling pathway to promote LN metastasis of BCa. Furthermore, inactivating the TGF-β/SMAD3 signaling pathway using the TGFβR1 inhibitor LY364947 eliminated the circEHBP1-mediated increase in VEGF-D expression. Collectively, our study expanded our knowledge of the role played by TGFβR1 in the LN metastasis of BCa.

Recent reports have identified circRNAs as promising targets for clinical application due to their abundance, high stability, and unique expression pattern.[13,14,40] Endogenous circRNAs from the host and exogenous circRNAs encoded by viruses contribute to the prevention of viral infections.[41] Nonetheless, little is known about the potential therapeutic role played by circRNAs in patients with BCa with LN metastasis. In the present study, we demonstrated that circEHBP1 was highly expressed in samples from patients with BCa with LN metastasis. Additionally, we found that circEHBP1 overexpression effectively promoted popliteal LN metastasis in nude mice, indicating that circEHBP1 was a potential therapeutic target for LN metastasis in BCa. Thus, circEHBP1 facilitates LN metastasis in BCa and represents a new target for intervention strategies to treat LN metastasis in patients with BCa.

### Conclusions

In summary, we revealed a novel pathway in which circEHBP1 increases the secretion of VEGF-D to facilitate lymphangiogenesis and LN metastasis in BCa, independent of VEGF-C. Clinically, circEHBP1 overexpression correlated closely with LN metastasis. Our study supports circEHBP1 as a potential biomarker and therapeutic target for LN metastasis in patients with BCa.

## MATERIALS AND METHODS

Additional materials and methods can be found in the Supplemental information.

### Clinical samples and ethics statement

In the present study, 186 pairs of tumor tissues and NATs from patients with BCa who underwent surgery were obtained at Sun Yat-sen Memorial Hospital from March 2012 to July 2018. For RNA extraction, the clinical samples were quickly frozen in liquid nitrogen and stored at −80°C. For IHC, the samples were fixed in 10% neutral-buffered formalin, then dehydrated with 70% ethanol, and finally embedded in paraffin. Tumor staging was performed according to the latest version of the tumor node metastasis (TNM) system from the American Joint Committee on Cancer. The collection of human tissue requires the informed consent of the patient and the approval of the Ethics Committee of the Sun Yat-sen Memorial Hospital, Sun Yat-sen University (approval number: 2015[034]). Three experienced pathologists independently affirmed the histological and pathological diagnoses of each sample.

### Cell culture

The human BCa cell lines (UM-UC-3, T24, and 5637) and SV-HUC-1 were acquired from the ATCC (Manassas, VA, USA). UM-UC-3

**Figure 5. circEHBP1 attenuates miR-130a-3p-mediated *TGFBR1* suppression**

(A–D) Representative images and quantification of tube formation and Transwell migration by HLECs that were cultured with the supernatant obtained from miR-130a-3p-silencing (A and B), miR-130a-3p-overexpressing (C and D), or control UM-UC-3 and T24 cells. Scale bars, 100 μm. (E) Schematic illustrating the sequence alignment of miR-130a-3p with the 3′ UTR of TGFβR1. (F and G) The luciferase activities of the TGFβR1-3′ UTR-wt plasmid or TGFβR1-3′ UTR-mut plasmid quantified following transfection with the NC mimic or miR-130a-3p mimics in UM-UC-3 (F) and T24 (G) cells. (H and I) Quantitative real-time RT-PCR analysis of the effect of circEHBP1 knockdown (H) or circEHBP1 overexpression (I) on *TGFBR1* expression in UM-UC-3 and T24 cells. (J) The effect of circEHBP1 knockdown on miR-130a-3p depletion-induced TGFβR1 promotion in UM-UC-3 and T24 cells was analyzed by quantitative real-time RT-PCR. (K and L) Western blotting analysis of the effect of circEHBP1 knockdown on miR-130a-3p depletion-induced TGFβR1 expression in UM-UC-3 (K) and T24 (L) cells. (M–P) Western blotting assay showing the levels of TGFβR1, SMAD3, and p-SMAD3 after circEHBP1 knockdown (M and N) or circEHBP1 overexpression (O and P) in UM-UC-3 and T24 cells. Two-tailed Student's t test or 1-way analyses of variance were used to determine the significance level, and Dunnett's test was used for multiple comparisons. Error bars indicate the standard deviations. *$p < 0.05$, **$p < 0.01$.

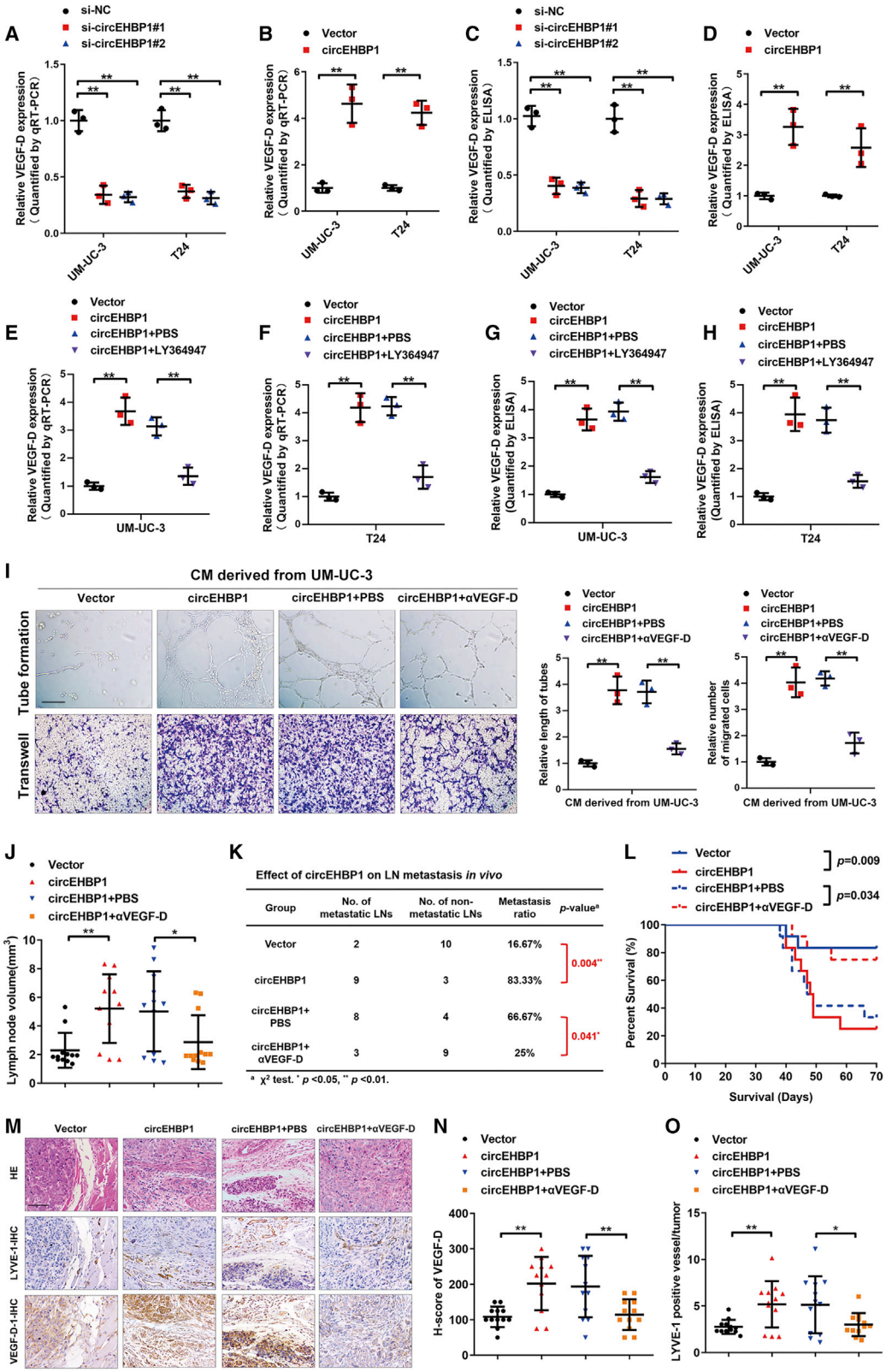


(legend on next page)

cells were maintained in Dulbecco's modified Eagle's medium (DMEM) (Gibco, Carlsbad, CA, USA), T24 and 5637 cells were cultured in 1640 medium (Gibco), and SV-HUC-1 cells were cultured in F-12K medium (Wisent, Saint-Jean-Baptiste, QC, Canada). All media were supplemented with 10% fetal bovine serum (FBS; HyClone, Logan, UT, USA). HLECs were obtained from ScienCell Research Laboratories and maintained in ECM (Gibco), which contained 5% FBS. All cells were maintained at 37°C in a humidified incubator with 5% $CO_2$.

### Popliteal lymphatic metastasis assay

All animal studies were carried out according to our previously published guidelines[42] and permitted by Sun Yat-sen Memorial Hospital, Sun Yat-sen University. Nude BALB/c mice at 4 to 5 weeks old were obtained from the Experimental Animal Center (Guangzhou, P.R. China). The mice were divided randomly into groups, and $5 \times 10^6$ UM-UC-3 cells transfected with circEHBP1-overexpressing vector or negative control (NC) vector were inoculated into the right footpad of each mouse. When the tumor reached 200 $mm^3$, the mice were visualized using the IVIS spectral imaging system; the primary tumor and popliteal LNs were removed and then analyzed by IHC using anti-LYVE-1 antibodies (Abcam, Cambridge, UK). Images were visualized under a Nikon Eclipse Ti microscope (Nikon, Japan). Original images of excised popliteal LNs from the nude mice are shown in Figure S5.

### Biotin-coupled probe RNA pull-down assay

To prepare the streptavidin-coated magnetic beads, the beads were blocked with 10 μg/μL bovine serum albumin (BSA) and yeast tRNA for 3 h on a rotator at 4°C and then incubated with an oligo probe or circEHBP1 probe for 2 h at room temperature. About $2 \times 10^7$ UM-UC-3 or T24 cells were immobilized with 1% formaldehyde and lysed with lysis buffer, and then the beads containing pulldown probes were incubated with cell lysates overnight. Next, 50 μL of cell lysate was extracted as input, and quantitative real-time RT-PCR analysis was performed for target gene calculation. The probes used in the assay are shown in Table S4.

### Further applied methods

Additional plasmids and siRNA transfection, lentiviral transduction, RNA preparation, quantitative real-time RT-PCR, IHC, gel electrophoresis analysis, RNase R treatment, northern blotting, actinomycin D experiment, CCK-8 and colony formation assay, HLEC tube formation assay, Transwell assay, nuclear and cytoplasmic fractionation experiment, FISH, co-localization of circEHBP1 and miR-130a-3p, dual-luciferase reporter assay, and ELISA are further described in the Supplemental methods. The antibodies used in this study are shown in Table S5.

### Data Availability

RNA-sequence data have been deposited in the GEO database and can be accessed with GEO: GSE77661.

### Statistical analysis

All statistical data are presented as the mean ± standard deviation from three experiments independently using GraphPad Prism version 8.0 (GraphPad, La Jolla, CA, USA). Kaplan-Meier analysis and the log-rank test were performed to assessed survival. The $\chi^2$ test was used to analyze the connection between circEHBP1 and the pathological parameters of patients with BCa. The differences in parameter variables between the two groups were estimated using two-tailed Student's t test or 1-way analysis of variance (ANOVA). A probability below 0.05 was used as an indicator of statistical significance.

## SUPPLEMENTAL INFORMATION

Supplemental Information can be found online at https://doi.org/10.1016/j.ymthe.2021.01.031.

## ACKNOWLEDGMENTS

This research was funded by the National Natural Science Foundation of China, China (grant nos. 81672395, 81871945, 81802530, and 82072639); the National Key Research and Development Project of China, China (grant no. 2017YFC1308600); the Guangdong Science and Technology Department, China (grant nos. 2020A1515010815 and 2017A020215072); the Science and Technology Program of Guangzhou, China (grant nos. 202002030388, 201803010049, and 201704020097); the Yixian Youth project of Sun Yat-sen Memorial Hospital, China (grant no. YXQH201812); and the Young Teacher Training Funding of Sun Yat-sen University, China (grant no. 19ykpy121).

## AUTHOR CONTRIBUTIONS

J.Z., C.C., and Z.L. participated in the study design. J.Z., Y. Luo, and Y.Z. conducted the *in vitro* and *in vivo* experiments. Y.K., Y. Li, and H.Z. performed the data analyses. B.G. and L.A. conducted the clinical data analyses. Y. Li, Y.Z., and J.H. performed the IF and IHC

**Figure 6. circEHBP1 elevates VEGF-D expression via activating the TGF-β/SMAD3 signaling pathway**

(A and B) Quantitative real-time RT-PCR analysis of the impact of circEHBP1 knockdown (A) or circEHBP1 overexpression (B) on the *VEGFD* expression in UM-UC-3 and T24 cells. (C and D) ELISA analysis of the impact of circEHBP1 knockdown (C) or circEHBP1 overexpression (D) on VEGF-D secretion in UM-UC-3 and T24 cells. (E and F) Quantitative real-time RT-PCR analysis of the treatment effect of LY364947 on circEHBP1-overexpressing-induced *VEGFD* expression in UM-UC-3 (E) and T24 (F) cells. (G and H) ELISA analysis of the treatment effect of LY364947 on circEHBP1-overexpressing-induced VEGF-D secretion in UM-UC-3 (G) and T24 (H) cells. (I) Representative images and quantification of tube formation and Transwell migration by HLECs that were cultured with the supernatant obtained from UM-UC-3 cell with vector, circEHBP1-overexpressing, circEHBP1-overexpressing+PBS, and circEHBP1-overexpressing +αVEGF-D. Scale bar, 100 μm. (J) The measurement of the LN volume in the indicted groups. (K) The popliteal LN metastatic rate in all groups (n = 12). (L) Kaplan-Meier survival curves in all groups (n = 12). (M–O). Representative images (M) and histogram analysis (N and O) of IHC staining showing the effects of VEGF-D neuralization on circEHBP1-induced VEGF-D expression and the quantities of lymphatic vessels in footpad tumors. Scale bar, 50 μm. Two-tailed Student's t test or 1-way analyses of variance were used to determine the significance level, and Dunnett's test was used for multiple comparisons. Error bars indicate standard deviations. *$p < 0.05$, **$p < 0.01$.

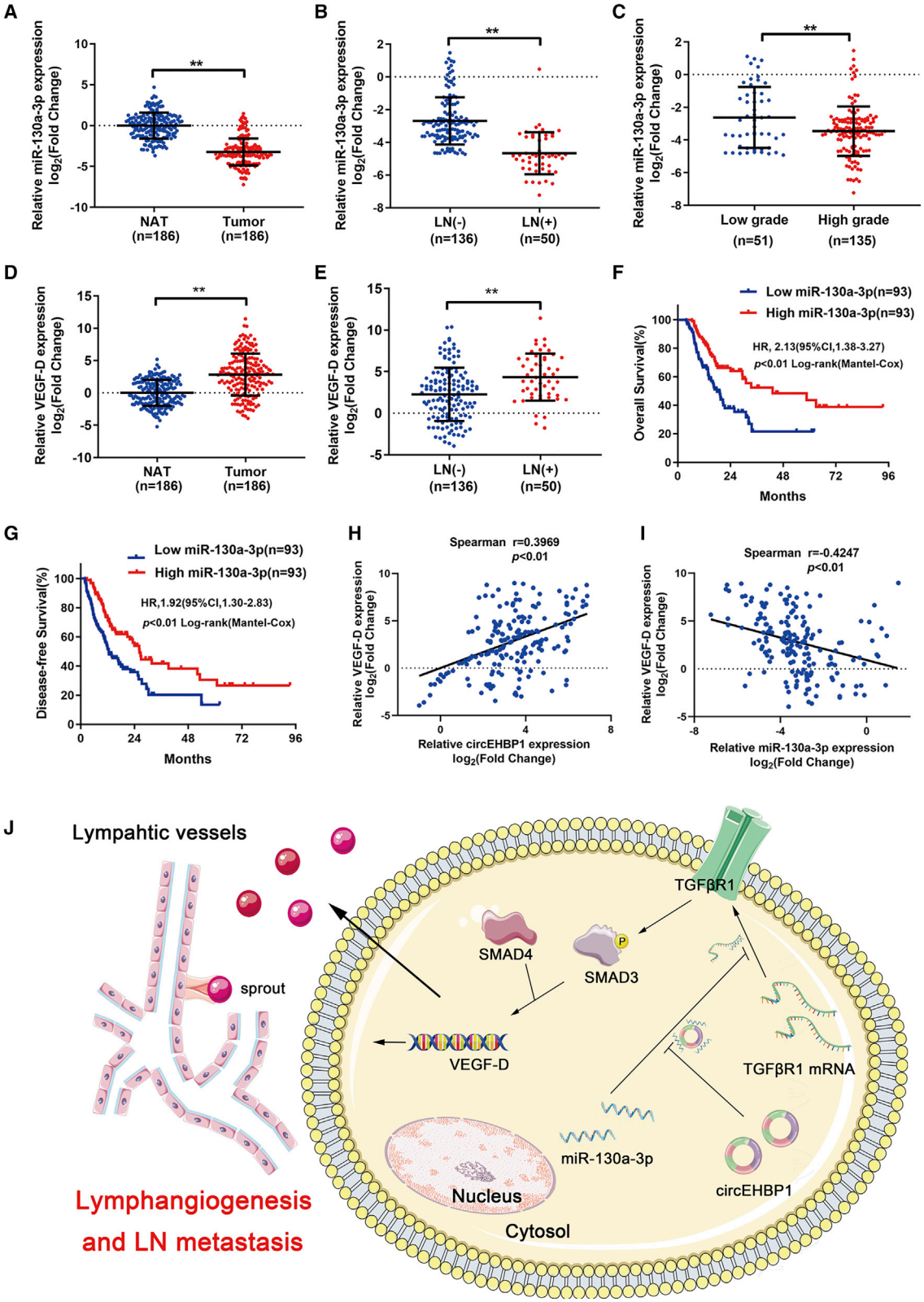


*(legend on next page)*

experiments. J.Z., Y. Luo, and C.C. wrote the manuscript. All authors have read and approved of the final manuscript.

## DECLARATION OF INTERESTS

The authors declare no competing interests.

## REFERENCES


1. Patel, V.G., Oh, W.K., and Galsky, M.D. (2020). Treatment of muscle-invasive and advanced bladder cancer in 2020. CA Cancer J. Clin. *70*, 404–423.
2. Hautmann, R.E., de Petriconi, R.C., Pfeiffer, C., and Volkmer, B.G. (2012). Radical cystectomy for urothelial carcinoma of the bladder without neoadjuvant or adjuvant therapy: long-term results in 1100 patients. Eur. Urol. *61*, 1039–1047.
3. Xie, R., Chen, X., Cheng, L., Huang, M., Zhou, Q., Zhang, J., Chen, Y., Peng, S., Chen, Z., Dong, W., et al. (2021). NONO Inhibits Lymphatic Metastasis of Bladder Cancer via Alternative Splicing of SETMAR. Mol. Ther. *29*, 291–307.
4. Stacker, S.A., Williams, S.P., Karnezis, T., Shayan, R., Fox, S.B., and Achen, M.G. (2014). Lymphangiogenesis and lymphatic vessel remodelling in cancer. Nat. Rev. Cancer *14*, 159–172.
5. Sundar, S.S., and Ganesan, T.S. (2007). Role of lymphangiogenesis in cancer. J. Clin. Oncol. *25*, 4298–4307.
6. Jussila, L., and Alitalo, K. (2002). Vascular growth factors and lymphangiogenesis. Physiol. Rev. *82*, 673–700.
7. Stacker, S.A., Caesar, C., Baldwin, M.E., Thornton, G.E., Williams, R.A., Prevo, R., Jackson, D.G., Nishikawa, S., Kubo, H., and Achen, M.G. (2001). VEGF-D promotes the metastatic spread of tumor cells via the lymphatics. Nat. Med. *7*, 186–191.
8. Karnezis, T., Shayan, R., Caesar, C., Roufail, S., Harris, N.C., Ardipradja, K., Zhang, Y.F., Williams, S.P., Farnsworth, R.H., Chai, M.G., et al. (2012). VEGF-D promotes tumor metastasis by regulating prostaglandins produced by the collecting lymphatic endothelium. Cancer Cell *21*, 181–195.
9. Colak, S., and Ten Dijke, P. (2017). Targeting TGF-β Signaling in Cancer. Trends Cancer *3*, 56–71.
10. Liao, Z., Chen, L., Zhang, X., Zhang, H., Tan, X., Dong, K., Lu, X., Zhu, H., Liu, Q., Zhang, Z., et al. (2020). PTPRε Acts as a Metastatic Promoter in Hepatocellular Carcinoma by Facilitating Recruitment of SMAD3 to TGF-β Receptor 1. Hepatology *72*, 997–1012.
11. Yang, H., Fang, F., Chang, R., and Yang, L. (2013). MicroRNA-140-5p suppresses tumor growth and metastasis by targeting transforming growth factor β receptor 1 and fibroblast growth factor 9 in hepatocellular carcinoma. Hepatology *58*, 205–217.
12. Calon, A., Espinet, E., Palomo-Ponce, S., Tauriello, D.V., Iglesias, M., Céspedes, M.V., Sevillano, M., Nadal, C., Jung, P., Zhang, X.H., et al. (2012). Dependency of colorectal cancer on a TGF-β-driven program in stromal cells for metastasis initiation. Cancer Cell *22*, 571–584.
13. Li, J., Sun, D., Pu, W., Wang, J., and Peng, Y. (2020). Circular RNAs in Cancer: Biogenesis, Function, and Clinical Significance. Trends Cancer *6*, 319–336.
14. Wu, Q., Liu, W., Wang, J., Zhu, L., Wang, Z., and Peng, Y. (2020). Exosomal noncoding RNAs in colorectal cancer. Cancer Lett. *493*, 228–235.
15. Guo, X., Zhou, Q., Su, D., Luo, Y., Fu, Z., Huang, L., Li, Z., Jiang, D., Kong, Y., Li, Z., et al. (2020). Circular RNA circBFAR promotes the progression of pancreatic ductal adenocarcinoma via the miR-34b-5p/MET/Akt axis. Mol. Cancer *19*, 83.
16. Sang, Y., Chen, B., Song, X., Li, Y., Liang, Y., Han, D., Zhang, N., Zhang, H., Liu, Y., Chen, T., et al. (2019). circRNA_0025202 Regulates Tamoxifen Sensitivity and Tumor Progression via Regulating the miR-182-5p/FOXO3a Axis in Breast Cancer. Mol. Ther. *27*, 1638–1652.
17. Zheng, Q., Bao, C., Guo, W., Li, S., Chen, J., Chen, B., Luo, Y., Lyu, D., Li, Y., Shi, G., et al. (2016). Circular RNA profiling reveals an abundant circHIPK3 that regulates cell growth by sponging multiple miRNAs. Nat. Commun. *7*, 11215.
18. He, W., Zhong, G., Jiang, N., Wang, B., Fan, X., Chen, C., Chen, X., Huang, J., and Lin, T. (2018). Long noncoding RNA BLACAT2 promotes bladder cancer-associated lymphangiogenesis and lymphatic metastasis. J. Clin. Invest. *128*, 861–875.
19. Suzuki, K., Morita, T., and Tokue, A. (2005). Vascular endothelial growth factor-C (VEGF-C) expression predicts lymph node metastasis of transitional cell carcinoma of the bladder. Int. J. Urol. *12*, 152–158.
20. Li, Z., Qi, F., Miao, J., Zu, X., He, W., Wang, L., and Qi, L. (2010). Vascular endothelial growth factor-C associated with computed tomography used in the diagnosis of lymph node metastasis of bladder carcinoma. Arch. Med. Res. *41*, 606–610.
21. Zhong, Y., Du, Y., Yang, X., Mo, Y., Fan, C., Xiong, F., Ren, D., Ye, X., Li, C., Wang, Y., et al. (2018). Circular RNAs function as ceRNAs to regulate and control human cancer progression. Mol. Cancer *17*, 79.
22. Zhou, C., Liu, H.S., Wang, F.W., Hu, T., Liang, Z.X., Lan, N., He, X.W., Zheng, X.B., Wu, X.J., Xie, D., et al. (2020). circCAMSAP1 Promotes Tumor Growth in Colorectal Cancer via the miR-328-5p/E2F1 Axis. Mol. Ther. *28*, 914–928.
23. Chang, T.H., Huang, H.Y., Hsu, J.B., Weng, S.L., Horng, J.T., and Huang, H.D. (2013). An enhanced computational platform for investigating the roles of regulatory RNA and for identifying functional RNA motifs. BMC Bioinformatics *14* (*Suppl 2*), S4.
24. Agarwal, V., Bell, G.W., Nam, J.W., and Bartel, D.P. (2015). Predicting effective microRNA target sites in mammalian mRNAs. eLife *4*, e05005.
25. Huang, H.Y., Lin, Y.C., Li, J., Huang, K.Y., Shrestha, S., Hong, H.C., Tang, Y., Chen, Y.G., Jin, C.N., Yu, Y., et al. (2020). miRTarBase 2020: updates to the experimentally validated microRNA-target interaction database. Nucleic Acids Res. *48* (D1), D148–D154.
26. Pian, C., Zhang, G., Gao, L., Fan, X., and Li, F. (2020). miR+Pathway: the integration and visualization of miRNA and KEGG pathways. Brief. Bioinform. *21*, 699–708.
27. Mori, M.A., Ludwig, R.G., Garcia-Martin, R., Brandão, B.B., and Kahn, C.R. (2019). Extracellular miRNAs: From Biomarkers to Mediators of Physiology and Disease. Cell Metab. *30*, 656–673.
28. Kong, Y., Li, Y., Luo, Y., Zhu, J., Zheng, H., Gao, B., Guo, X., Li, Z., Chen, R., and Chen, C. (2020). circNFIB1 inhibits lymphangiogenesis and lymphatic metastasis via the miR-486-5p/PIK3R1/VEGF-C axis in pancreatic cancer. Mol. Cancer *19*, 82.
29. Astin, J.W., Haggerty, M.J., Okuda, K.S., Le Guen, L., Misa, J.P., Tromp, A., Hogan, B.M., Crosier, K.E., and Crosier, P.S. (2014). Vegfd can compensate for loss of Vegfc in zebrafish facial lymphatic sprouting. Development *141*, 2680–2690.
30. Fernández, M.I., Bolenz, C., Trojan, L., Steidler, A., Weiss, C., Alken, P., Grobholz, R., and Michel, M.S. (2008). Prognostic implications of lymphangiogenesis in muscle-invasive transitional cell carcinoma of the bladder. Eur. Urol. *53*, 571–578.
31. Haiko, P., Makinen, T., Keskitalo, S., Taipale, J., Karkkainen, M.J., Baldwin, M.E., Stacker, S.A., Achen, M.G., and Alitalo, K. (2008). Deletion of vascular endothelial growth factor C (VEGF-C) and VEGF-D is not equivalent to VEGF receptor 3 deletion in mouse embryos. Mol. Cell. Biol. *28*, 4843–4850.


**Figure 7. Clinical significance of circEHBP1 inducing miR-130a-3p/*TGFBR1*/VEGF-D axis in patients with BCa**

(A) Quantitative real-time RT-PCR for the miR-130a-3p level among a 186-case cohort of BCa tissues paired with corresponding NATs. The Mann-Whitney U test was employed. (B and C) Quantitative real-time RT-PCR analysis of miR-130a-3p levels among 186 cases of BCa with respect to LN status (B) and pathological grade (C). The Mann-Whitney U test was employed. (D) Quantitative real-time RT-PCR for the VEGF-D expression in a 186-case cohort of BCa tissues paired with corresponding NATs. The Mann-Whitney U test was employed. (E) Quantitative real-time RT-PCR analysis of VEGF-D expression in 186 cases of BCa according to LN status. The Mann-Whitney U test was employed. (F and G) Kaplan-Meier survival curves for OS (F) and DFS (G) of low miR-130a-3p versus high miR-130a-3p level in patients with BCa. The median expression of miR-130a-3p was taken as the cutoff value. (H) Quantitative real-time RT-PCR for the correlation of circEHBP1 and VEGF-D expression in 186 cases of BCa. (I) Quantitative real-time RT-PCR for the correlation of miR-130a-3p and VEGF-D expression in 186 cases of BCa. (J) Schematic illustrating the potential mechanism of circEHBP1 on lymphangiogenesis and LN metastasis facilitation in BCa via the miR-130a-3p/TGFβR1/VEGF-D axis. Error bars indicate standard deviations. *$p < 0.05$, **$p < 0.01$.

32. Morfoisse, F., Tatin, F., Hantelys, F., Adoue, A., Helfer, A.C., Cassant-Sourdy, S., Pujol, F., Gomez-Brouchet, A., Ligat, L., Lopez, F., et al. (2016). Nucleolin Promotes Heat Shock-Associated Translation of VEGF-D to Promote Tumor Lymphangiogenesis. Cancer Res. *76*, 4394–4405.

33. Orlandini, M., Marconcini, L., Ferruzzi, R., and Oliviero, S. (1996). Identification of a c-fos-induced gene that is related to the platelet-derived growth factor/vascular endothelial growth factor family. Proc. Natl. Acad. Sci. USA *93*, 11675–11680.

34. Karnezis, T., Farnsworth, R.H., Harris, N.C., Williams, S.P., Caesar, C., Byrne, D.J., Herle, P., Macheda, M.L., Shayan, R., Zhang, Y.F., et al. (2019). CCL27/CCL28-CCR10 Chemokine Signaling Mediates Migration of Lymphatic Endothelial Cells. Cancer Res. *79*, 1558–1572.

35. Hong, H., Jiang, L., Lin, Y., He, C., Zhu, G., Du, Q., Wang, X., She, F., and Chen, Y. (2016). TNF-alpha promotes lymphangiogenesis and lymphatic metastasis of gallbladder cancer through the ERK1/2/AP-1/VEGF-D pathway. BMC Cancer *16*, 240.

36. Wang, X., Chen, X., Meng, Q., Jing, H., Lu, H., Yang, Y., Cai, L., and Zhao, Y. (2015). MiR-181b regulates cisplatin chemosensitivity and metastasis by targeting TGFβR1/Smad signaling pathway in NSCLC. Sci. Rep. *5*, 17618.

37. Qiao, Y., Wang, Z., Tan, F., Chen, J., Lin, J., Yang, J., Li, H., Wang, X., Sali, A., Zhang, L., and Zhong, G. (2020). Enhancer Reprogramming within Pre-existing Topologically Associated Domains Promotes TGF-β-Induced EMT and Cancer Metastasis. Mol. Ther. *28*, 2083–2095.

38. Wang, S., Huang, M., Wang, Z., Wang, W., Zhang, Z., Qu, S., and Liu, C. (2019). MicroRNA-133b targets TGFβ receptor I to inhibit TGF-β-induced epithelial-to-mesenchymal transition and metastasis by suppressing the TGF-β/SMAD pathway in breast cancer. Int. J. Oncol. *55*, 1097–1109.

39. Gore, J., Imasuen-Williams, I.E., Conteh, A.M., Craven, K.E., Cheng, M., and Korc, M. (2016). Combined targeting of TGF-β, EGFR and HER2 suppresses lymphangiogenesis and metastasis in a pancreatic cancer model. Cancer Lett. *379*, 143–153.

40. Zhang, M., and Xin, Y. (2018). Circular RNAs: a new frontier for cancer diagnosis and therapy. J. Hematol. Oncol. *11*, 21.

41. Awan, F.M., Yang, B.B., Naz, A., Hanif, A., Ikram, A., Obaid, A., Malik, A., Janjua, H.A., Ali, A., and Sharif, S. (2021). The emerging role and significance of circular RNAs in viral infections and antiviral immune responses: possible implication as theranostic agents. RNA Biol. *18*, 1–15.

42. Chen, C., He, W., Huang, J., Wang, B., Li, H., Cai, Q., et al. (2018). LNMAT1 promotes lymphatic metastasis of bladder cancer via CCL2 dependent macrophage recruitment. Nat. Commun. *9*, 3826.